NASA Technical Memorandum 103964

Sol-Gel Synthesis and Densification of Aluminoborosilicate Powders Part 1–Synthesis

Jeffrey Bull, Guna Selvaduray, and Daniel Leiser

September 1992

National Aeronautics and Space Administration

NASA Technical Memorandum 103964

Sol-Gel Synthesis and Densification of Aluminoborosilicate Powders Part 1–Synthesis

Jeffrey Bull, Ames Research Center, Moffett Field, California
Guna Selvaduray, San Jose State University, San Jose, California
Daniel Leiser, Ames Research Center, Moffett Field, California

September 1992

National Aeronautics and
Space Administration

Ames Research Center
Moffett Field, California 94035-1000

SOL-GEL SYNTHESIS AND DENSIFICATION OF ALUMINOBOROSILICATE POWDERS PART I–SYNTHESIS

Jeffrey Bull, Guna Selvaduray,* and Daniel Leiser
Ames Research Center

Summary

Aluminoborosilicate powders high in alumina content were synthesized by the sol-gel process utilizing various methods of preparation. Properties and microstructural effects related to these syntheses were examined. After heating to 600°C for 2 h in flowing air the powders were amorphous with the metal oxides comprising 87% of the weight and uncombusted organics the remainder. DTA of dried powders revealed a T_g at approximately 835°C and an exotherm near 900°C due to crystallization. Powders derived from aluminum secbutoxide consisted of particles with a mean diameter 5μm less than those from aluminum isopropoxide. Powders synthesized with aluminum isopropoxide produced agglomerates comprised of rod shaped particulates while powders made with the secbutoxide precursor produced irregular glassy shards. Compacts formed from these powders required different loadings for equivalent densities according to the method of synthesis.

Introduction

The sol-gel process is a low temperature chemical synthesis which uses solutions, sols, or mixtures of both as a precursor for glass and ceramic materials (ref. 1). The process is most commonly used to produce single component and multi-component hydroxylated gels. Products obtained from these gels include but are not limited to bulk glasses, fibers, thin films, and powders (ref. 2). The application of this process to the production of powders in the alumina-boria-silica (ABS) system is the topic of this paper.

The Al_2O_3·B_2O_3·SiO_2 system phase diagram is shown in figure 1 (ref. 3). The vaporization of B_2O_3 (boria) at elevated temperatures from this system makes compositional control difficult. Referring to the composition indicated by "N" in figure 1, as boria volatilizes, additional mullite should precipitate from the solid solution of $3Al_2O_3{\cdot}2SiO_2$ and $9Al_2O_3{\cdot}2B_2O_3$. A decomposition reaction such as this has been observed in the temperature range of 1200–1400°C in ceramic fibers of similar composition (refs. 4 and 5).

As both of these compounds are refractory, with melting points in excess of 1800°C, fibers which contain them find use in high temperature applications where oxidizing enviroments are encountered. Nextel-312 is a commercially available ceramic fiber with the composition indicated by "N" (62 wt percent Al_2O_3· 14 wt percent B_2O_3· 24 wt percent SiO_2) in figure 1 which has considerable retention of mechanical strength for long durations at temperatures up to 1205°C in air (ref. 6). This fiber is currently used as an integral component of a family of low density insulative materials known as Fibrous Refractory Composite Insulation (FRCI) (ref. 7). FRCI is now used as a thermal protection material in selected areas on space shuttle Orbiters. As a component of FRCI, the Nextel fiber provides a boria source for promoting silica fiber-to-fiber bonding and decreases shrinkage at high temperatures. The overall strength of this composite is much greater than a comparable density all-silica insulation. Addition of the Nextel fiber not only reduces the processing temperature of the composite insulation but decreases the driving force for silica devitrification. At temperatures greater than the processing temperature of FRCI (≈1315°C) the rate of boria vaporization from the Nextel fiber increases with increasing temperature (ref. 5). This in turn decreases the effective or "apparent" viscosity of the composite and retards the devitrification of silica fibers to cristobalite (Dan Leiser, private communication, 1989). However, in these silica based composite insulations, it is disadvantageous to

*San Jose State University, San Jose, California.

have excess boria present after processing because reduced viscosity can degrade their dimensional stability at temperatures exceeding the processing temperature.

Therefore a means of tailoring the thermochemical behavior of materials in the ABS system with enhanced processing characteristics would prove most advantageous in extending the high temperature resistance of these insulations. Sol-gel processing of multicomponent oxides has been demonstrated by several authors (refs. 9–13) and may be suitable for high temperature use. This paper describes several methods of chemically synthesizing powders of a single composition within the ABS system via the sol-gel process, and the effect of those methods on the powder's physical properties.

We appreciate the generosity of Surface Science Laboratories, Mountain View, Calif., for performing the ESCA work.

Experimental

Two methods of synthesis were employed in using the sol-gel process to produce ABS powders and each method was accomplished using two different aluminum alkoxides. By altering the method of synthesis, the introduction of structural modifications at the molecular level should be expected in the early stages of polymerization. Further modifications should be induced by utilizing the different hydrolysis reactivities of the alumina precursors, as well as those of polymeric species subsequently formed in the sol.

Based on the composition indicated by "N" in figure 1, corresponding to a molar ratio of 3:1:2 for Al_2O_3:B_2O_3:SiO_2, reaction steps and mechanisms were proposed for the two methods of synthesis (method I and method II) as detailed in figures 2 and 3, respectively. These mechanisms are ideal in that they describe only well established paths to stable monomeric species. The actual mechanisms are undoubtedly more complex, with not only the formation of the shown monomers, but the formation of many dimeric, trimeric, and other intermediates as well. Nevertheless, the proposed mechanisms provide a necessary guide to the method of synthesis and the required stoichiometry.

The synthesis methods used were developed based on the work of Brinker and Mukherjee (ref. 8) as well as those of Yoldas (refs. 9 and 10) and Fleming (ref. 11)—all of which pertain to the chemical synthesis of multicomponent oxides. Each method was conducted with two different alumina precursors, with the alumina precursors extending each designation by an arabic numeral, i.e., the isopropoxide alumina precursor of method I is designated I.ABS.1 and the secbutoxide precursor of method II is II.ABS.2. Quantity, grade, and source of reagents used in the syntheses are listed in table 1.

Ethanol was used as the common solvent for all oxide precursors, their hydrolysis products, and water. In method I, an ethanolic solution of tetraethylorthosilicate (TEOS) was partially hydrolized and then an ethanolic solution of trimethyl borate (TMB) was added while stirring. This borosiloxane sol was then added to a slurry of AIP or ASB and vigorously stirred. Final hydrolysis of this mixture was performed by adding, dropwise, an aqueous ethanolic solution with additional stirring. Method II is similar to method I except that the alumina precursor is added prior to the boria precursor. An ethanolic solution of TMB was then added to the corresponding aluminosiloxane sol. This mixture was then hydrolyzed as in method I, producing sols with a concentration totalling 5 wt percent equivalent oxide. This concentration and the use of an acidic catalyst, HNO_3, were to encourage extensive polymerization and the formation of a network structure of the constituent oxides. All steps of the syntheses were performed in air at atmospheric pressure with no precautions taken to prevent premature hydrolysis from atmospheric moisture. The gelled material was dried in an air-circulated oven at 80°C for 24 to 48 h to give the powder. The powder was ground with a porcelain mortar and pestle and heated again at 600°C for 2 h in flowing air. These pre-calcined powders were sieved through a 80 mesh (180 μm) sieve. Agglomerates not able to pass through the sieve were ground until they passed freely through the sieve; only two passes were necessary. Powder compacts were made from the resultant material by dry pressing at variable loads in a carbon steel die, sprayed with zinc stearate as a die lubricant.

Powders obtained from the various methods were chemically analyzed using inductively coupled plasma atomic emission spectroscopy (ICP-AES) and electron spectroscopy for chemical analysis (ESCA). Thermochemical analysis was accomplished using thermogravimetric analysis (TGA) and differential thermal analysis (DTA). Particle size analysis, X-ray diffraction (XRD), and scanning electron microscopy (SEM),

were used for structural characterization. Apparent density of the powders and powder compacts was determined by volume pycnometry using helium as the working gas. Bulk density of the powder compacts was determined by mass and volume measurements.

Results and Discussion

Compositional Analysis

Chemical analysis of the ABS powders revealed slight deviations from the 3:1:2 ratio of Al_2O_3:B_2O_3:SiO_2, as shown in table 2. The largest deviations occurred in the Al_2O_3/SiO_2 ratio and are positive. The SiO_2/B_2O_3 ratio is nearest in agreement with the calculated ratio. Hence, the deviations are most likely due to depletion in the boria and silica content of the powder. The presence of Al, Si, and B as non-oxides, e.g., hydroxides, would also contribute to the relative errors. Preliminary results from ESCA indicated that the majority of the metals were present as oxides and so this contribution was negligible. Depletions in the silica content could be due to the vaporization of unreacted silanol species during drying and pre-calcination. Xiaoming and Yuguang (ref. 13) observed significant depletions in the boria content for an ABS system with alumina as the minor constituent and attributed this loss to hydrolysis of the TMB with atmospheric moisture. They showed that the compositional deviation increased with decreasing SiO_2/B_2O_3 molar ratio; the greatest deviation (88.9%) occurring at a ratio of 2.08, a ratio nearly equal to that described in this work. No depletions of this magnitude were found in these powders since the maximum value calculated was 6%. A minute adjustment in the quantity of TMB and TEOS was made to reduce the deviations. The values shown in tables 1–4 reflect this adjustment and are the mean values from synthesis of three batches.

Table 3 lists the major oxide constituents and their abundance in the pre-calcined powders. The values in this table show that all synthesized ABS powders are of equal composition. Approximately 13% of the weight is non-oxide material at this stage of processing. This mass difference was attributed to both residual organics and physically and chemically bound water. Table 4 lists the quantities of minor oxide constituents, impurities, detected in the initial batch of powders. It is obvious from this table that ABS powders based on the ASB precursor contain lower levels of impurities than those based on AIP. The difference was attributed to the initial purity of the alumina precursors.

The chemical composition of an ABS powder compact as determined by ICP-AES and ESCA are compared in table 5. The agreement is relatively good. ESCA shows that the mass difference previously observed is partially due to uncombusted carbon. High resolution techniques with ESCA in the vicinity of the peaks due to Al and Si show that these metals are present as oxides. The same technique shows B present as a mixture of oxide and hydroxide. This indicates either terminal linkages of boron in the polymer network or its failure to be incorporated into the network. The close agreement between the analytical values and the calculated value shows that the powder compacts are chemically homogeneous and consist primarily of the metal oxides.

Thermochemical Analysis

The dried ABS powders consisted of bleach-white particulates and agglomerates. Powders made with ASB took approximately twice as long to dry as those made with AIP. After pre-calcination, the powders varied in color from white to gray depending on the extent of oxidation of the organic constituents. Oxidation of residual organics and other weight loss phenomena were revealed in the thermal analysis of the synthesized powders.

Results of TGA of the dried powders are shown in figure 3. The curves of weight loss vs. temperature are all characterized by a rapid weight loss between 25 and 300°C followed by a gradual transition to a slower but more constant weight loss in the temperature range from 300–1000°C. This is followed by an increase in weight loss between 1000 and 1200°C. Between 40 and 53% of the initial powder weight was lost over the entire temperature range of 25–1200°C, although the total weight loss was dependent on the method of synthesis.

The initial rapid weight loss, between 30 and 35% of the total, was due to the elimination of trapped solvent and reaction by-products (H_2O and ROH) and desorption of excess water (refs. 8, 13, and 14). Figure 4 shows thermograms from DTA of the different

powders. In the temperature range from 25–100°C for this figure, a suppressed but nonetheless distinct endotherm was observed in all cases. These endotherms correspond to the range of high weight loss observed in figure 5 over the same temperature range. Endotherms in this temperature range are due to the loss of adsorbed water, and reaction by-products (methanol, ethanol, isopropanol, and secbutanol) from the hydrolysis of the alkoxides. Reaction by-product removal is particularly evident in the 100–200°C range by an inflection of those curves belonging to ASB based methods, i.e., I and II.ABS.2. This inflection, not present in the AIP based methods, is due to the lower vapor pressure of secbutanol relative to isopropanol resulting in a depressed rate of vaporization in the former. The exotherms at approximately 300°C in figure 5 are due to combustion of organics (CH_3O^-, $C_2H_5O^-$, etc.) (refs. 15 and 16). Hence, species such as $Si(OH)_x(OC_2H_5)_{4-x}$, $B(OH)_y(OCH_3)_{3-y}$, and $Al(OH)_z(OR)_{3-z}$, where R is either the isopropanol or secbutanol radical, exist up to this temperature at the stated heating rate. These exotherms occur in the transition region between high and low weight loss of figure 5 indicating that the majority of alkoxides have been converted to their equivalent oxide at this temperature. It was expected that the samples prepared from the higher molecular weight precursor (aluminum secbutoxide), i.e., I.ABS.2 and II.ABS.2, would lose more weight at this combustion point than those prepared from alumium isopropoxide. In figure 4 it can be seen that this is the case for powders prepared from method I but not so for method II.

The region of weight loss in the temperature range 300–1000°C is characterized by a slow but constant increase in weight loss due to additional condensation reactions (ref. 7). Hence, thermally soaking the green powders within this temperature range was considered a "pre-calcination" treatment.

There is no significant change in weight around 900°C and so the exotherms present in figure 5 near this temperature were attributed to a structural transformation. The change in slope of the DTA baseline at ≈835°C is common to all powders and indicative of a change in their specific heat capacity. Such a change occurs at the onset of the gel to glass transition, and hence, 835°C corresponds to the glass transition temperature (T_g) of the ABS powders. Xiaoming and Yuguang (ref. 12) reported a T_g of approximately 930°C for high silica bearing gels within the ABS system and a SiO_2/B_2O_3 = 3.93. Sowman (ref. 4) reported an exotherm in the DTA of aluminum borosilicate gels, similar in composition to those studied here, in the temperature range 850–870°C. His subsequent XRD analysis revealed the coincident formation of a novel crystalline species, a "reverse mullite," in this temperature range.

The increase in slope of the TGA curves in the temperature range 1000–1200°C accounted for an additional 1–5% weight loss. No thermal event was revealed in the corresponding temperature range of the DTA thermograms. The slopes are all similar with the exception of I.ABS.2 which is considerably greater (fig. 3). Reconciliation with other experimental results is necessary before suggesting a plausible origin for this anomaly.

Physical Properties and Structure

Physical property characterization of the powders and powder compacts began with their apparent density (ρ_a), i.e., density due to the solid phase and the isolated pores within the solid phase. It was assumed that the relative amounts of isolated pores were small compared to the continuous pores.

After drying, the powders had a mean apparent density equal to 1.72 g/cm^3. Individual values of the apparent densities for each synthesis method is given in table 6. The values of apparent density increased by ≈28% during pre-calcination. This increase indicated a considerable consolidation of the gel particulate during this stage of processing. This increase also corresponded with a decrease in volume large enough to offset the corresponding decrease in weight from 25–600°C as indicated by the TGA results of figure 2. The needed volume contraction could have occurred as a result of the polycondensation reactions within individual particles and agglomerates. The result of these reactions, occurring simultaneously with the expulsion of combustion and condensation reaction by-products, is the collapse of macropores in the gel resulting in a decreased porosity and a strengthening of the gel skeletal structure. The apparent density of the ABS powders after pre-calcination is approximately that of silica glass (2.20 g/cm^3) (ref. 17). This value was retained as the initial apparent density of the powder compacts.

The influence of the methods of synthesis was most significant in the particle size distribution and morphology. Table 7 lists the mean particle size and distribution and the mean diameter of agglomerates as analyzed by SEM imaging. Particle size analysis, determined after the powders were pre-calcined, showed that AIP based powders consisted of larger agglomerates but had a smaller mean particle size and distribution than those powders based on ASB. The particle distribution differed significantly between I.ABS.1 and I.ABS.2.

Figures 6(a) and (b) show an agglomerate from AIP and ASB based powders respectively, both having been exposed to 600°C for 2 h. The agglomerates from methods based on AIP were found to be more regularly shaped than those based on ASB. The later's agglomerates were more shard-like in shape. Figures 6(c) and (d) are a higher magnification of the enclosed region in the micrographs of figures 6(a) and (b), respectively. Figure 6(c) shows that the AIP based agglomerate is composed of submicron particulates as well as what appears to be well ordered rod-like structures. The ASB agglomerate shown in figure 4(d) revealed a featureless morphology common in many glasses (refs. 14 and 15). Hence, it appears that ABS particulates derived from ASB are richer in glass than those synthesized from AIP. XRD of all powders showed them to be amorphous at this stage of processing.

Powder Compaction

Powder compacts were formed from the pre-calcined powders.It was found that, for equal combinations of pressure and time, different densities resulted with compaction. This was considered to be detrimental for additional densification studies and hence powder compacts were formed based on an optimum green density of 45% relative to glass. The variation in relative bulk density (ρ/ρ_u), where ρ_u is the density of fused silica, with punch pressure for ABS powders is shown in figure 7. The required pressure needed to obtain the desired density could then be obtained by interpolation from this plot and ranged from 100–160 MPa (14.5–23.2 ksi). The pressure was applied to the sample for a total of five minutes in one minute stages.

The variation in compaction pressure correlates with the particle size and morphology of the pre-calcined powders. The smaller particles found in AIP based powders result in greater densities at lower applied pressures. Their agglomerates are also more easily comminuted with increasing pressure than those based on ASB.

The ABS green compacts were very tenacious and could be easily handled. The average dimensions of a green compact were 0.515 inches in diameter and 0.240 inches in thickness. These dimensions gave a thickness to diameter ratio of 0.47, a value indicative of minimal bulk density gradients in powder compacts pressed from a single action die (ref. 17).

Conclusions

Aluminoborosilicate powders with the molar ratio 3:1:2 (Al_2O_3:B_2O_3:SiO_2) were synthesized using the sol-gel process. Methods of synthesis were developed to show the potential for structural control as revealed by differences in thermochemical behavior, physical properties, and morphology.

After drying and pre-calcining (600°C for 2 h in flowing air) the powders, methods based on AIP resulted in powders with mean particle diameters 5μm less than those based on ASB. Powders synthesized from AIP produced regularly shaped agglomerates comprised of rod shaped crystallites, while those based on ASB formed glassy irregular shard-like agglomerates. However, all powders were amorphous after precalcination. Powder compaction behavior was reflective of these particle characteristics. Greater compact densities at lower compaction pressures were achieved with AIP based powders. A glass transition temperature of ≈835°C was common to all powders as well as an exotherm at approximately 900°C. This exotherm was attributed to a crystalline transformation. An increase in weight loss was observed above 1100°C and is believed to be due to the vaporization of boria. The temperature range and magnitude of the increase varied according to the method of synthesis.

ASB based powders contained less trace impurities than AIP based powders and was attributed to the chemical purity of the alumina precursor. No correlation between these contaminants and the characterized powders was evident.

References

1. Yoldas, B.: Preparation of Glasses and Ceramics from Metal-Organic Compounds. J. Mater. Sci., vol. 12, 1977, pp. 1203-8.

2. Fitzer, E.; and Gadow, R.: Fibre Reinforced Composites via the Sol/Gel Route. pp. 571-607 in Materials Science Research, Vol. 20, Tailoring Multiphase and Composite Ceramics. Edited by R. Tressler, G. Messing, C. Pantaro, and R. Newnham, Plenum Press, New York, 1986.

3. Gielisse, P.; and Foster, W.: Quart. Prog. Report 931-8, The Ohio State University Research Foundation, Oct., 1961, p. 6.

4. Sowman, H.: Alumina-Boria-Silica Ceramic Fibers from the Sol-Gel Process, Chapter 8, pp. 162-182 in Sol-Gel Technology for Thin Films, Fibers, Prefroms, Electronics and Specialty Shapes. Edited by Lisa C. Klein, Noyes Publications, New Jersey, 1988.

5. Sowman, H.: U.S. Patent No. 3,795,524, March 5, 1974; Minnesota Mining and Manufacturing Company.

6. Engineers' Guide to Composite Materials, Section 5. Edited by J. W. Weaton, D. M. Petters, and K. L. Thomas, ASM, 1987.

7. Leiser, D.; Smith, M.; and Stewart, D.: Options for Improving Rigidized Ceramic Heatshields. Ceram. Eng. Sci. Proc., vol. 6, nos. 7-8, 1985, pp. 757-68.

8. Brinker, C.; and Mukherjee, S.: Conversion of Monolithic Gels to Glasses in a Multicomponent Silicate Glass System. J. Mater. Science, vol. 16, 1981, pp. 1980-88.

9. Yoldas, B.: Monolithic Glass Formation by Chemical Polymerization. J. Mater. Sci., vol. 14, 1979, pp. 1843-49.

10. Yoldas, B.: Microstructure of Monolithic Materials Formed by Heat Treatment of Chemically Polymerized Precursors in the $Al_2O_3-SiO_2$ Binary. Ceram. Bull., vol. 59, no. 4, 1980, pp. 479-83.

11. Fleming, J.: Sol-Gel Processing of Glass Powders. pp. 155-161 in Advances in Ceramics, Vol. 21, Ceramic Powder Science, 1987.

12. Xiaoming, L.; and Yuguang, W.: Some Characteristics of Glass in the $Al_2O_3-B_2O_3-SiO_2$ System from the Gel. J. Non-Cryst. Solids, vol. 80, 1986, pp. 564-70.

13. Hoffman, D.; Roy, R.; and Komarneni, S.: Diphasic Xerogels, a New Class of Materials: Phases in the System $Al_2O_3-SiO_2$, J. Am. Ceram. Soc., vol. 67, 1984, pp. 468-71.

14. Carturan, G.; Gottardi, V.; and Graziani, M.: Physical and Chemical Evolutions Occurring in Glass Formation from Alkoxides of Silicon, Aluminum, and Sodium. J. Non-Cryst. Solids, vol. 29, 1978, pp. 41-48.

15. Holland, W.; Plumant, E., and Duvigneaud, P.: Crystallization of $SiO_2-Al_2O_3-MgO$ Glasses. J. Non-Cryst. Solids, vol. 48, 1982, pp. 205-17.

16. Tohge, N.; Moore, G.; and Mackenzie, J.: Structural Developments during the Gel to Glass Transition. J. Non-Cryst. Solids., vol. 63, 1984, pp. 95-103.

17. Schmidt, H.; and Scholze, H.: Mechanisms and Kinetics of the Hydrolysis and Condensation of Alkoxides. pp. 263-280 in Glass...Current Issues. Edited by A. F. Wright and J. Dupuy, Martinus Nijhoff Publishers, Dordrecht, The Netherlands, 1985.

Table 1. Grade and supplier of reagents used in the synthesis of ABS powders

Reagent	Designated grade	Supplier
Aluminum *iso*-propoxide $Al(OC_3H_7)_3$	98 + %	Alfa Products
Aluminum tri-(*sec*-butoxide) $Al(OC_4H_9)_3$	Double distilled	Chattem Chemicals
Teraethylorthosilicate $Si(OC_2H_5)_4$	Reagent	Fisher Scientific Co.
Trimethyl borate $B(OCH_3)_3$	Practical	Eastman Kodak Co.
Ethyl alcohol C_2H_5OH	U.S.P.	U.S. Industrial Chemicals Co.
Water H_2O	Distilled and deionized > 18 megaohm	Barnstead Co.
Nitric acid HNO_3	78% Baker Instra-Analyzed	J.T. Baker Chemical Co.

Table 2. Comparison of calculated and analyzed molar oxide ratios in synthesized ABS powders after pre-calcination

Method	Oxide molar ratio		
	Al_2O_3/SiO_2	Al_2O_3/B_2O_3	SiO_2/B_2O_3
I.ABS.1	1.69	3.18	1.88
I.ABS.2	1.64	3.18	1.94
II.ABS.1	1.69	3.18	1.88
II.ABS.2	1.64	3.37	2.06
Calculated	1.50	3.00	2.00

Table 3. Major oxide concentrations in synthesized ABS powders after pre-calcination

Method	Oxide (wt percent)			
	Al_2O_3	B_2O_3	SiO_2	otal
I.ABS.1	55.4	12.0	19.7	87.1
I.ABS.2	55.4	12.4	20.1	87.9
II.ABS.1	55.4	11.7	19.3	86.4
II.ABS.2	54.6	11.0	20.0	85.6
Calculated	62.0	14.0	24.0	100.0

Table 4. Impurity levels in synthesized ABS powders after pre-calcination

Method	Impurity concentration (wt percent)					
	Na_2O	K_2O	Li_2O	M_gO	CaO	Fe_2O_3
I.ABS.1	±LQD	0.26[a]	±LQD	0.015	0.007[a]	0.004[a]
I.ABS.2	±LQD	0.18[a]	±LQD	±LQD	0.007[a]	±LQD
II.ABS.1	±LQD	0.26[a]	±LQD	0.015	0.007[a]	0.003[a]
II.ABS.2	±LQD	0.24[a]	±LQD	0.015	0.005[a]	±LQD

Note. All results have an accuracy of ±1% except where indicated.
LQD = Lowest quantity determinable.
[a]Values are ±10% of that reported.

Table 5. Calculated and analyzed chemical composition of an ABS powder compact as determined by ESCA and ICP-AES

Element	Atom percent			Analytical
	Calculated	ESCA[a]	ICP-AES[b]	agreement, atom percent
Al	23.1	24.2	23.2	1.0
B	7.7	6.0	6.6	0.6
Si	7.7	9.6	7.0	2.4
C		3.7	4.4[d]	0.7
O	61.5	56.5	58.8[c]	2.3

[a]I.ABS.1 after 100 Å ion milling, probe area = 600 μm^2.
Accuracy is reported to be 10% of the relative abundance.
[b]I.ABS.1, accuracy of ±1% of reported value.
[c]Calculated from stoichiometric oxide content of listed metals.
[d]Difference from mass balance.

Table 6. Apparent density of synthesized ABS powders after several stages of processing

Method	Apparent density (g/cm^3)		
	Powder after 70°C, 24-48 h	Powder after 600°C, 2 h	Powder compact as pressed
I.ABS.1	1.68	2.15	2.24
I.ABS.2	1.67	2.28	2.09
II.ABS.1	1.87	2.18	2.16
II.ABS.2	1.67	2.22	2.15

Table 7. Particle size, distribution, and agglomerate diameter of synthesized ABS powders[a]

Method	Particle size (μm)	Particle distribution (μm)		Agglomerate diameter (μm)
		$\leq 95v/o$	$\leq 5v/o$	
I.ABS.1	9.5	34.6	2.2	53
I.ABS.2	15.31	43.5	2.5	46
II.ABS.1	8.9	39.5		53
II.ABS.2	12.7	41.9	2.9	40

[a]Determination of particle size and disribution based on laser diffraction using Rosin-Rammler distribution function and a measuring range of 1.86-135 μm. Agglomerate mean diameters from SEM imaging.

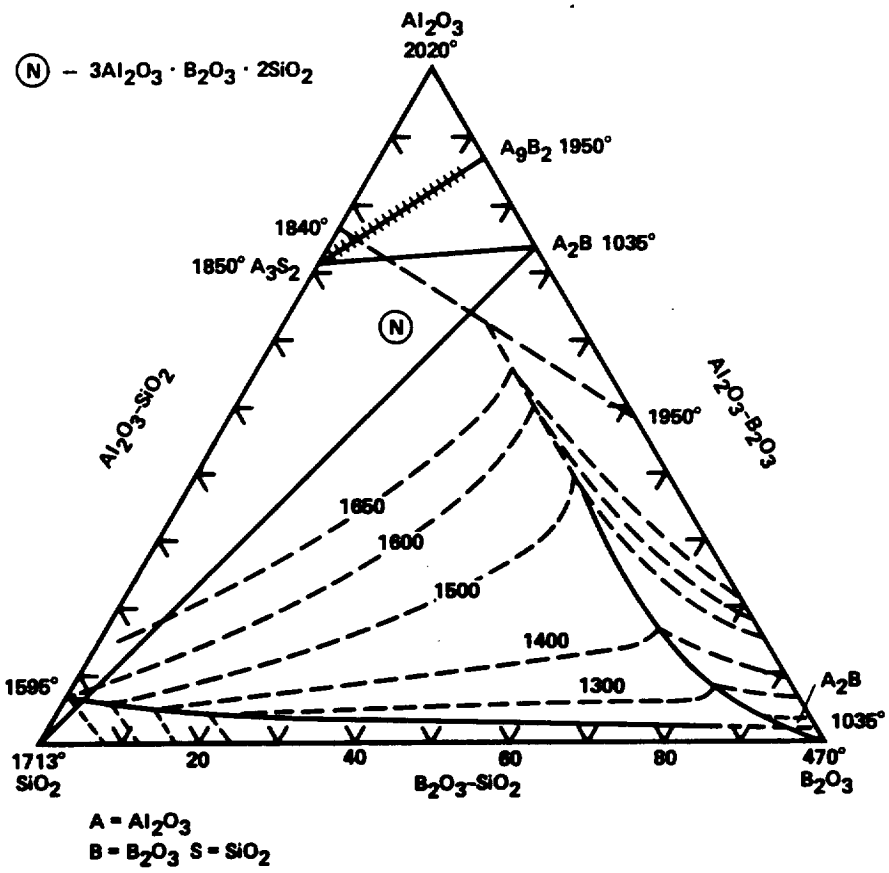

Figure 1. Al_2O_3·B_2O_3·SiO_2 phase diagram indicating the studied composition N.

Step	Reaction mechanism[a]
1.	$Si(OEt)_4 + H_2O \longrightarrow Si(OH)(OEt)_3 + EtOH$
2.	$Si(OH)(OEt)_3 + B(OMe)_3 \longrightarrow (EtO)_3SiOB(OMe)_2 + MeOH$
3.	$3Al(OR)_3 + (EtO)_3SiOB(OMe)_2 + 14H_2O \longrightarrow 3Al(OH)_3 + (HO)_3SiOB(OH)_2 + 9ROH + 3EtOH + 2MeOH$
4.	$6Al(OH)_3 + 2(HO)_3SiOB(OH)_2 \longrightarrow 3Al_2O_3 \cdot B_2O_3 \cdot 2SiO_2 + 14H_2O$

[a]R = $(C_3H_7)^{iso}$ for I.ABS.1 and $(C_4H_9)^{sec}$ for I.ABS.2, EtOH = C_2H_5OH, MeOH = CH_3OH.

Figure 2. Proposed reaction steps and mechanisms in the synthesis of ABS powders, method I.

Step	Reaction mechanism[a]
1.	$Si(OEt)_4 + H_2O \longrightarrow Si(OH)(OEt)_3 + EtOH$
2.	$Si(OH)(OEt)_3 + 3Al(OR)_3 \longrightarrow (EtO)_3SiOAl(OR)_2 + 2Al(OR)_3 + ROH$
3.	$(EtO)_3SiOAl(OR)_2 + 2Al(OR)_3 + B(OMe)_3 + 14H_2O \longrightarrow (HO)_3SiOAl(OH)_2 + 2Al(OH)_3 + B(OH)_3 + 3EtOH + 8ROH + 3MeOH$
4.	$2(HO)_3SiOAl(OH)_2 + 4Al(OH)_3 + 2B(OH)_3 \longrightarrow 3Al_2O_3 \cdot B_2O_3 \cdot 2SiO_2 + 14H_2O$

[a]R = $(C_3H_7)^{iso}$ for II.ABS.1 and $(C_4H_9)^{sec}$ for II.ABS.2, EtOH = C_2H_5OH, MeOH = CH_3OH.

Figure 3. Proposed reaction steps and mechanisms in the synthesis of ABS powders, method II.

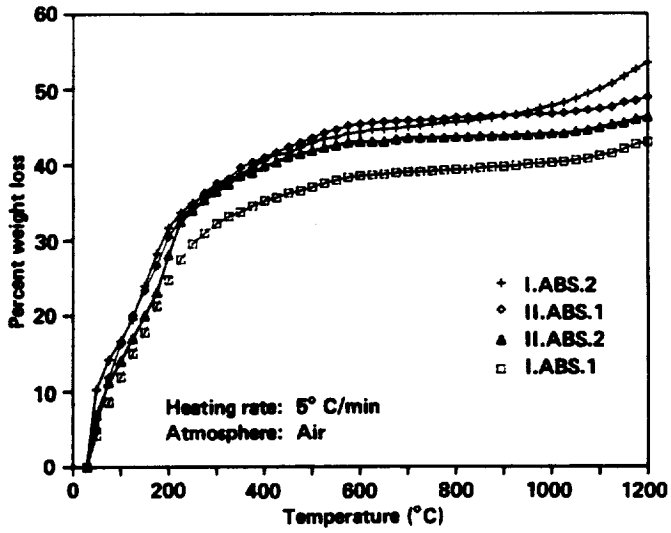

Figure 4. Percent weight loss with temperature from TGA of synthesized ABS powders.

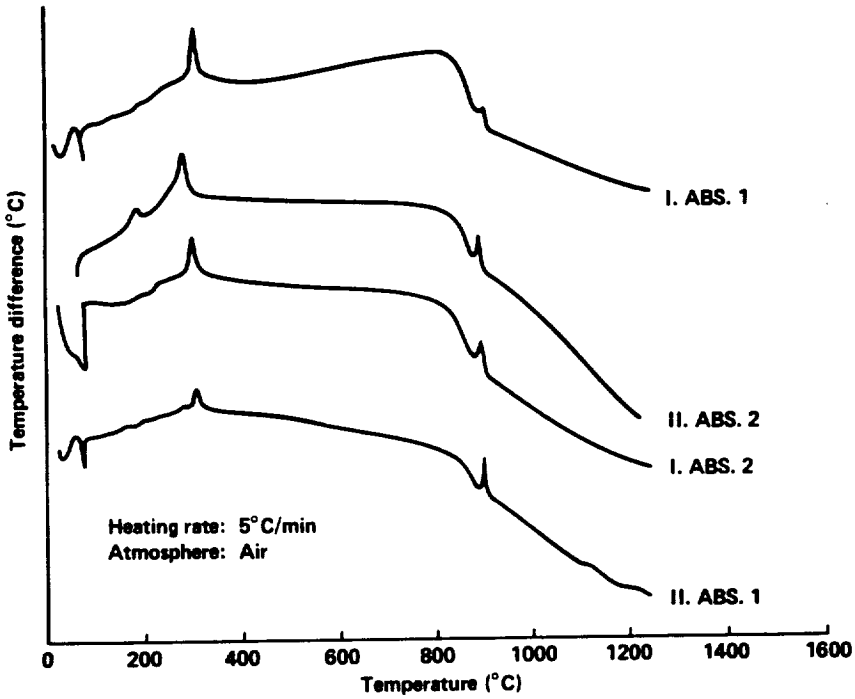

Figure 5. Temperature difference vs. temperature, from DTA of synthesized ABS powders.

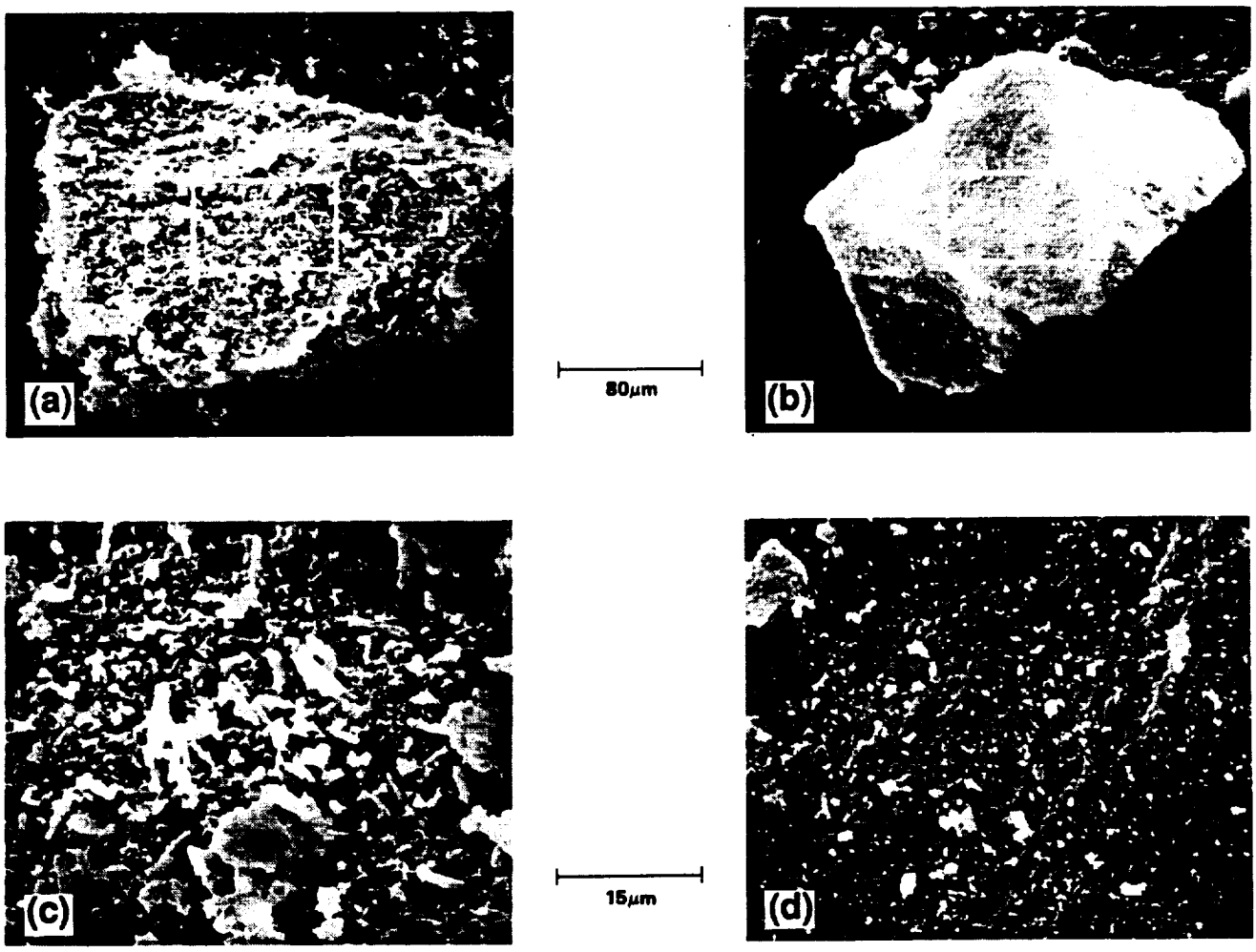

Figure 6. SEM micrograph of ABS agglomerates prepared from different methods. (a) AIP based agglomerate, (b) ASB based agglomerate, (c) 5X magnification of boxed area in (a); (d) 5X magnification of boxed area in (b).

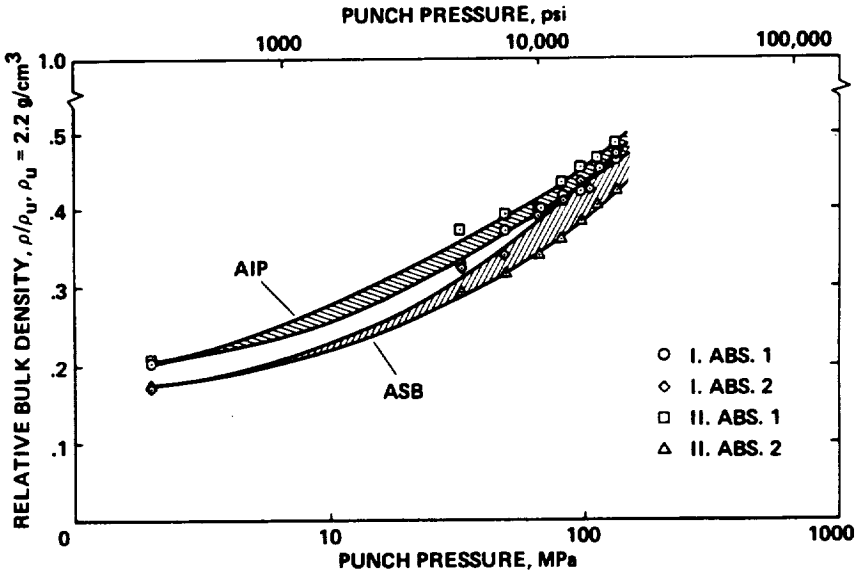

Figure 7. Variation in relative bulk density with compaction pressure for synthesized ABS powders.

REPORT DOCUMENTATION PAGE

Form Approved
OMB No. 0704-0188

1. AGENCY USE ONLY *(Leave blank)*	2. REPORT DATE	3. REPORT TYPE AND DATES COVERED
	September 1992	Technical Memorandum

4. TITLE AND SUBTITLE

Sol-Gel Synthesis and Densification of Aluminoborosilicate Powders. Part 1–Synthesis

5. FUNDING NUMBERS

506-43-31

6. AUTHOR(S)

Jeffrey Bull, Guna Selvaduray (San Jose State University, San Jose, CA), and Daniel Leiser

7. PERFORMING ORGANIZATION NAME(S) AND ADDRESS(ES)

Ames Research Center
Moffett Field, CA 94035-1000

8. PERFORMING ORGANIZATION REPORT NUMBER

A-92107

9. SPONSORING/MONITORING AGENCY NAME(S) AND ADDRESS(ES)

National Aeronautics and Space Administration
Washington, DC 20546-0001

10. SPONSORING/MONITORING AGENCY REPORT NUMBER

NASA TM-103964

11. SUPPLEMENTARY NOTES

Point of Contact: Jeffrey Bull, Ames Research Center, MS 234-1, Moffett Field, CA 94035-1000
(415) 604-5377

12a. DISTRIBUTION/AVAILABILITY STATEMENT

Unclassified-Unlimited
Subject Category – 23

12b. DISTRIBUTION CODE

13. ABSTRACT ***(Maximum 200 words)***

Aluminoborosilicate powders high in alumina content were synthesized by the sol-gel process utilizing various methods of preparation. Properties and microstructural effects related to these syntheses were examined. After heating to 600°C for 2 h in flowing air the powders were amorphous with the metal oxides comprising 87% of the weight and uncombusted organics the remainder. DTA of dried powders revealed a T_g at approximately 835°C and an exotherm near 900°C due to crystallization. Powders derived from aluminum secbutoxide consisted of particles with a meandiameter 5μm less than those from aluminum isopropoxide. Powders synthesized with aluminum isopropoxide produced agglomerates comprised of rod shaped particulates while powders made with the secbutoxide precursor produced irregular glassy shards. Compacts formed from these powders required different loadings for equivalent densities according to the method of synthesis.

14. SUBJECT TERMS

Aluminoborosilicate, Powders, Sol-gel, Chemical synthesis, Glass

15. NUMBER OF PAGES

14

16. PRICE CODE

A02

17. SECURITY CLASSIFICATION OF REPORT	18. SECURITY CLASSIFICATION OF THIS PAGE	19. SECURITY CLASSIFICATION OF ABSTRACT	20. LIMITATION OF ABSTRACT
Unclassified	Unclassified		